doi:10.36487/ACG_repo/2435_Q-02

Subsidence analysis of the SW Sector at El Teniente mine

C. Cancino[a], C. Alvarez[b] and R. Jara[c]
[a]*Itasca Minneapolis, USA*
[b]*Itasca Santiago, Chile*
[c]*El Teniente Division CODELCO, Chile*

ABSTRACT

El Teniente Mine (DET) has been developed through the years using the panel caving method, resulting in a notorious subsidence crater at the surface. Since 2011, operations related to an open pit named "Rajo Sur" took place in the southern sector adjacent to the subsidence crater, resulting in operational interference with the underground mine. In 2019, a new open pit called "Extension Norte Rajo Sur" (ENRS) was being planned in the southwestern sector, mostly within caved material. Assessing the potential interaction with the underground operation was key for the open pit project. Estimations of the active subsidence became pivotal for strategic project planning, particularly in determining the transition timing between underground and surface mining. A geomechanical assessment of the surface subsidence was carried out through numerical modeling to support the development of the economical pit of ENRS by estimating the expected topography over the years. The model was calibrated to site observations for the 2012–2018 period in terms of cave propagation, subsidence advance, and topographic vertical changes. Subsequently, a predictive analysis for the period 2018–2025 was conducted. This paper describes the numerical assessment, calibration and main assumptions made to assess the surface subsidence at El Teniente Mine for the period 2012–2025 and compares predictions with the actual current topography available today, finding a good overall agreement.

1 INTRODUCTION

El Teniente Mine (DET) is an underground copper mine located in the Andes range in the central zone of Chile, about 70 km southeast of Santiago. This mine has been developed for the last one hundred years using the panel caving method, resulting in a prominent subsidence crater at the surface. Operational challenges arose when the adjacent southern sector underwent open pit activities known as "Rajo Sur" since 2011, leading to interference with underground mining operations, with waste material being dumped into the active crater (Cancino et al., 2019). The planning of a new open pit, "Extension Norte Rajo Sur" (ENRS), mostly within the crater of caved material in the southwestern sector from 2019, necessitated a better understanding of the subsidence induced by active cave mining. Assessing the potential interaction with the underground operation was key for the open pit project. Estimations of the active subsidence became pivotal for strategic project planning, particularly in determining the transition timing between underground and surface mining.

This paper presents a 3D numerical assessment to support the development of the ENRS project by estimating the predictive active subsidence. Calibration of the model involved aligning it with site observations from 2012 to 2018, encompassing cave propagation, surface cave extension, and topographic vertical changes. Subsequently, a predictive analysis for the period of 2019–2025 was conducted. Since then, caving has taken place for more than 4 years (2019–2022). The key results presented here correspond to the comparison of the "predictive" model with observed current crater behavior up to 2022. This is a valuable exercise as it provides the opportunity to carry out a validation process beyond the initial calibration carried out for the analysis. As shown later, the comparison is reasonable, and the approach is suitable for the estimation of the advance of the active subsidence but holds some challenges when capturing the topographic vertical changes within the crater.

The following sections detail the numerical assessment, calibration process, and key assumptions underlying the evaluation of surface subsidence at El Teniente Mine.

2 NUMERICAL MODELING

2.1 Caving Numerical Model

Five key geomechanical zones are associated with caving, as shown in the conceptual model sketched in Figure 1. This builds on the conceptual model developed by Duplancic and Brady (1999).

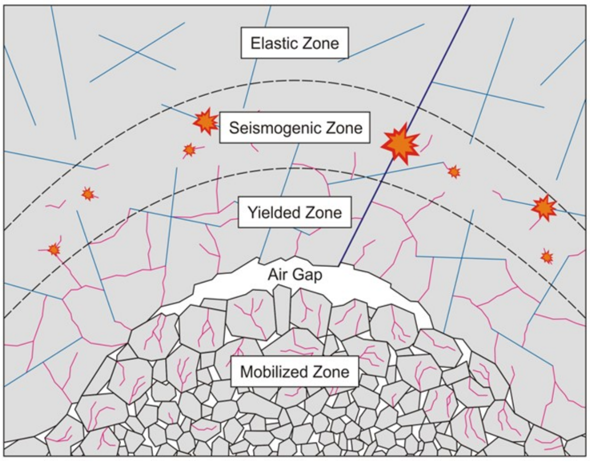

Figure 1 Conceptual model of caving (after Duplancic and Brady, 1999).

The numerical caving model, developed by Itasca in the context of the MMT project (Board and Pierce, 2009; Sainsbury, 2012), aims to replicate key aspects of the conceptual caving model, focusing on the progressive disintegration of the rock during the transition from intact to caved material. This is achieved using a strain-softening material, with strain-dependent properties adjusted to represent the impacts of dilation and bulking that accompany caving within the overall *FLAC3D* model (Itasca, 2023a).

Employing the proprietary strain-softening *Cave-Hoek* constitutive model in *FLAC3D*, the caving algorithm enables the representation of essential mechanisms such as modulus softening, density adjustment, dilation, cohesion and tension weakening, and frictional strengthening.

Specification of the drawpoint layout and schedule is accomplished through external ASCII files. The caving algorithm follows a rigorous mass-balance routine to ensure that the tons-based production schedule is represented accurately.

Undercutting is simulated by converting the model elements that represent the undercut to fully fragmented and bulked rock. The undercut volume is then deleted and the support to the surrounding rock mass is replaced with equivalent boundary forces that exist after the undercut is replaced by fragmented bulked rock. Ore draw is emulated by applying a minor downward velocity to all gridpoints in the roof of the undercut, maintained at a level low enough to ensure pseudo-static equilibrium across the entire model. The undercut progresses, and ore draw is simulated in incremental computational steps until reaching the target mass stipulated by the production schedule. As the mass is drawn from the undercut, the yielded zone spontaneously emerges within the *FLAC3D* model, determined by the stress state and yield strength of the rock mass, potentially advancing upward from the undercut. With continued draw, rock within the yielded zone displaces a sufficient distance to be recognized as caved (mobilized) material. Figure 2 shows the caving limit definitions in accordance with the conceptual model.

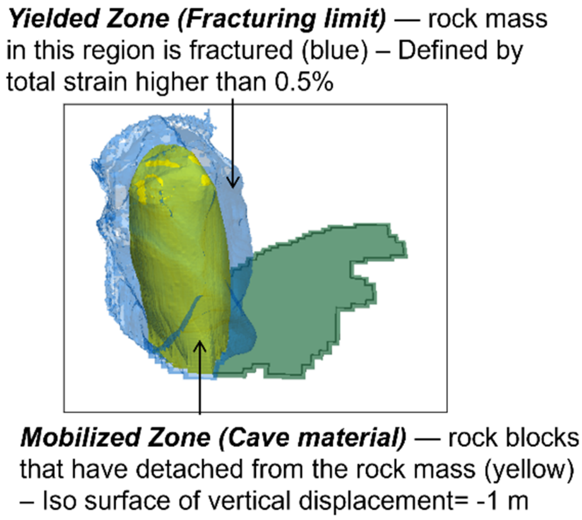

Figure 2 Caving limits from numerical model.

The cratering process involves monitoring the vertical displacement of the first layer of zones beneath a free surface. Upon reaching a vertical displacement value equal to its edge length, a zone is considered to have cratered and is consequently removed from the model. This cratering algorithm provides a certain level of predictability regarding the height and shape of the crater at any given point during the cave's lifespan. Figure 3 illustrates the formation and growth of a crater above a 100-m deep cave. This methodology has demonstrated success in calibrating numerous operations globally and specifically at the El Teniente mine (Alvarez et al., 2014; Cancino et al., 2019).

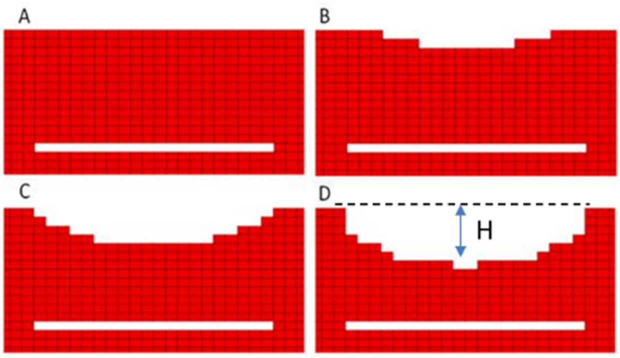

Figure 3 Example of a crater growing above a 100-m deep cave uniformly drawn.

3 MODEL CALIBRATION

Since all geomechanical analyses involving rock mass strength rely on empirical relations to estimate strength, it is prudent to calibrate strengths through back-analysis of actual site experience when available.

3.1 Background information

A back analysis was performed for site observations of a 7-year period at DET (2012 to 2018) in the southwestern sector of the mine (potential location for ENRS).

For the calibration process, topographical information was used considering the broken rock material (inside the crater) and crater limit (defined by field observations) representing the mobilize zone in Figure 2. The topographical information was obtained through aero-photogrammetric flights, which are made annually at DET, as well as measurements of displacements through geotechnical monitoring equipment.

3.1.1 Underground mining

Figure 4 illustrates in plan view the main information for the analyses. Since the mining site has been active for more than 100 years, the calibration considers an initial cave volume representing mining until 2011 (initial crater boundary shown by the yellow line in Figure 4). As shown in Figure 4, the active panels relevant for the ENRS project correspond to Pipa Norte (PN), Diablo Regimiento (DR), and Pacifico Superior (PS), with PN and DR being active prior to December 2011, and PS starting production during 2016, with an intact rock column of approximately 400 m. Information about the underground production program is given in Figure 5. Note that the production for 2018 was not actual but projected. The calibration simulates the production from year 2012 to 2018 (annually for the first 4 years, semesterly for 2016 and 2017, and quarterly for 2018) in the three active sectors pertinent to the ENRS project.

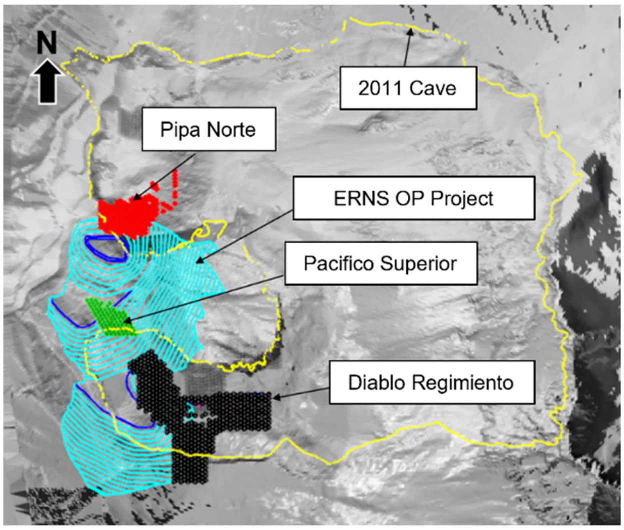

Figure 4 Plan view showing active drawpoints relevant to ENRS open pit project (2012–2017).

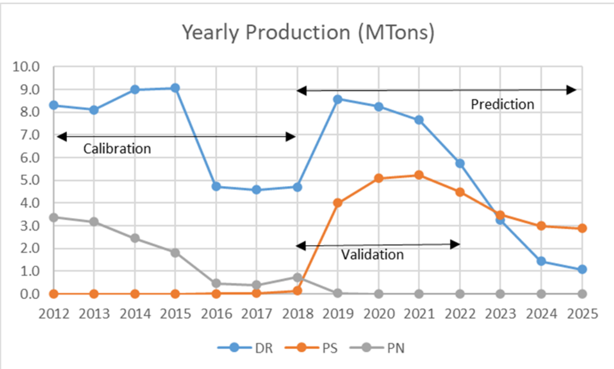

Figure 5 Yearly production program used in analyses.

The calibration was aimed at reproducing three aspects of mining evolution: the cave propagation rate of PS panel within in-situ rock mass, subsidence advance, and topographic vertical changes (cratering).

3.1.2 Geotechnical units

The predominant lithology corresponds to El Teniente Mafic Complex (CMET or Andesites) divided in two zones, called CMET hanging wall (Hw) and CMET footwall (Fw), which have been characterized to have different mechanical behavior (Pardo, 2015). At DET, there is a clear differentiation between primary and secondary rock, the first one being competent rock and the secondary being relatively weaker (Brzovic, 2010). Figure 6 shows the special distribution of the main units within the primary rock.

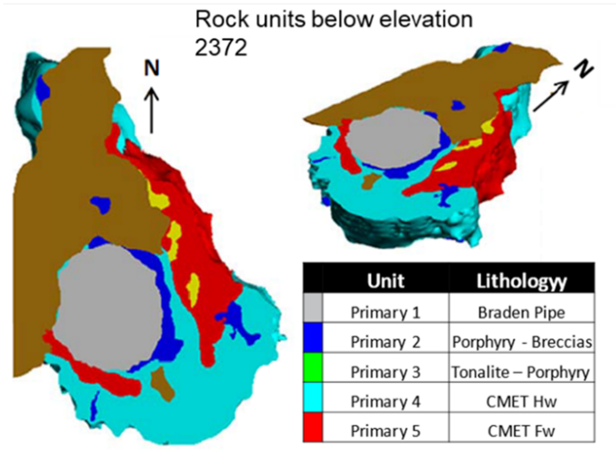

Figure 6 Plan and isometric views showing primary rock characterizations.

3.1.3 Intact and rock mass strength

The rock mass strength properties were provided initially by DET in terms of standard rock mass parameters (density, UCS, GSI, and mi) for each geotechnical unit. As shown later, GSI values of some of the units were adjusted during the calibration stage. The pre-existing cave material was represented by residual strength corresponding to a fully bulked rockfill (i.e., almost zero cohesion and friction angle of 40–45 deg). The intact and peak rock mass properties are summarized in Table 1.

3.1.4 In-situ stress regime

In 2015, DET carried out a mine-scale stress calibration by using numerical modeling, and the results are shown in Figure 7. The in-situ stresses were one of the most relevant inputs for the numerical model describe here.

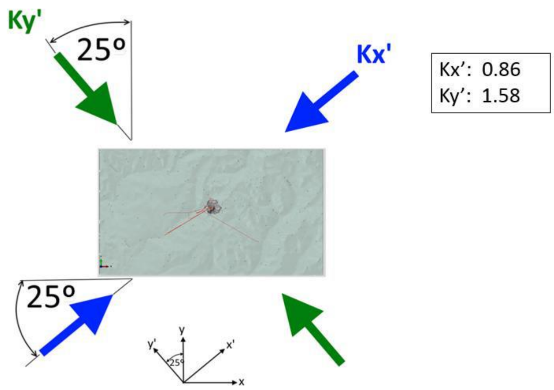

Figure 7 In-situ stress calibration results (DET, 2015).

Table 1 Property Summary

Unit	Sigci (MPa)	GSI	mi	Density (kg/m^3)	Ei (GPa)
Primary 1	74	60	7.5	2600	23
Primary 2	144	59	17	2680	39
Primary 3	151	52	14	2770	48
Primary 4 *	132	43 (48)	10.7	2770	57
Primary 5 *	108	41 (46)	10	2770	55
Sec CMET	60	33	10.7	2590	57
Sec Tonalite	70	50	6.2	2590	15
Sec Pipe *	74	40 (33)	7.5	2590	23

(*) Adjusted units with original values within brackets.

3.2 FLAC3D model

The *FLAC3D* model constructed to simulate underground mining is shown in Figure 8 (in green the pre-existing cave), representing a localized model for the crater, only around the area relevant to the open pit project. The smallest element size is 10 m in the region of interest. The initial model was run to equilibrium after assigning the rock mass properties, the in-situ stresses, and after initializing the existing cave. Note that the stresses inside the cave were initialized to zero to represent the presence of broken (therefore mobilized) material.

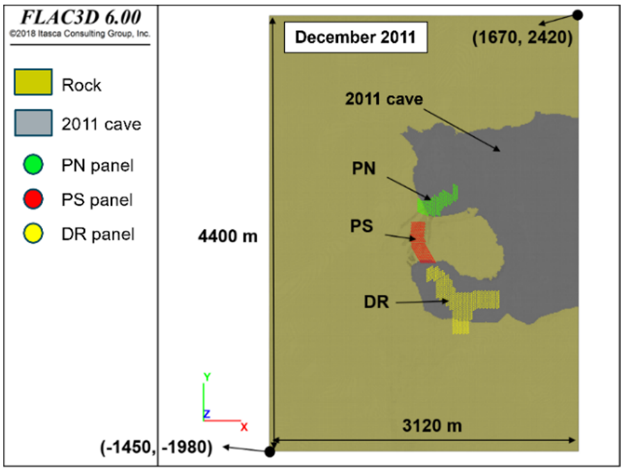

Figure 8 Plan view of the *FLAC3D* model.

The inclusion of the available structural model was key to back-analyze the cave initiation and propagation of the PS panel. Figure 9 shows a NS cross-section through the PS with the location of faults (in red) relative to the PS extraction panel and the pre-existing cavity. The faults are considered only outside of the imposed pre-existing cave.

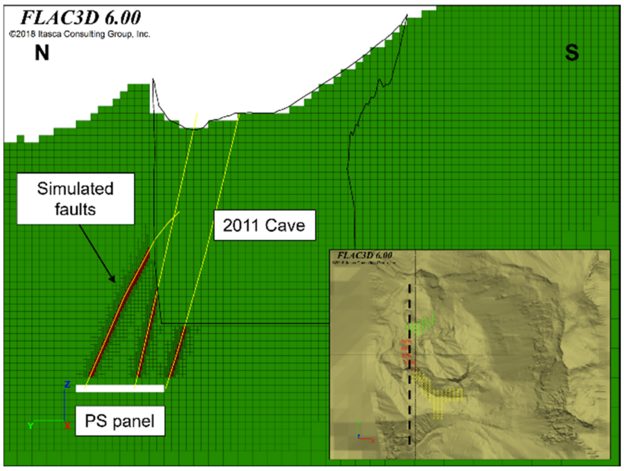

Figure 9 NS cross-section showing the existing faults near PS panel.

3.3 Cave Propagation

The propagation rates were studied via the connection time of the PS panel to the 2011 pre-existing cave and breakthrough surface. During Q2-2018, signs of surface subsidence were observed due to PS mining. Initial simulations resulted in slower propagation than observed in the site (later breakthrough). This is due to the rock mass pre-conditioning used by DET in the primary rock units. To account for this effect, it was necessary to reduce the shear strength of the relevant units for PS mining. Figure 10 shows the rock units across a NS section through the PS panel. The PS ore column shows the presence of Primary 4 (Tonalite) and Primary 5 (CMET Fw and Tourmaline Breccia), and Secondary CMET. It was necessary to reduce the GSI by 5 points of both primary units (see Table 1) to accelerate the propagation and meet the site observations.

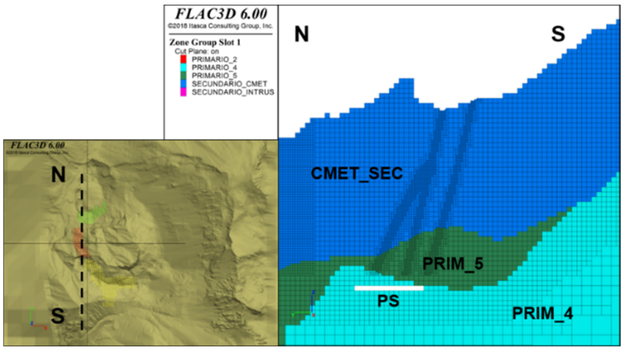

Figure 10 **NS cross-section showing rock units present in the PS ore column (PS panel in white).**

Figure 11 shows the calibrated PS cave propagation, with the green shape being the 2011 pre-existing cave, and the yellow shape the mobilized limit of the simulated mining (see Figure 2). The PS interaction with the pre-existing cave happened at the end of Q1-2018 and the breakthrough to surface during Q2-2018, showing a good overall agreement with site observations.

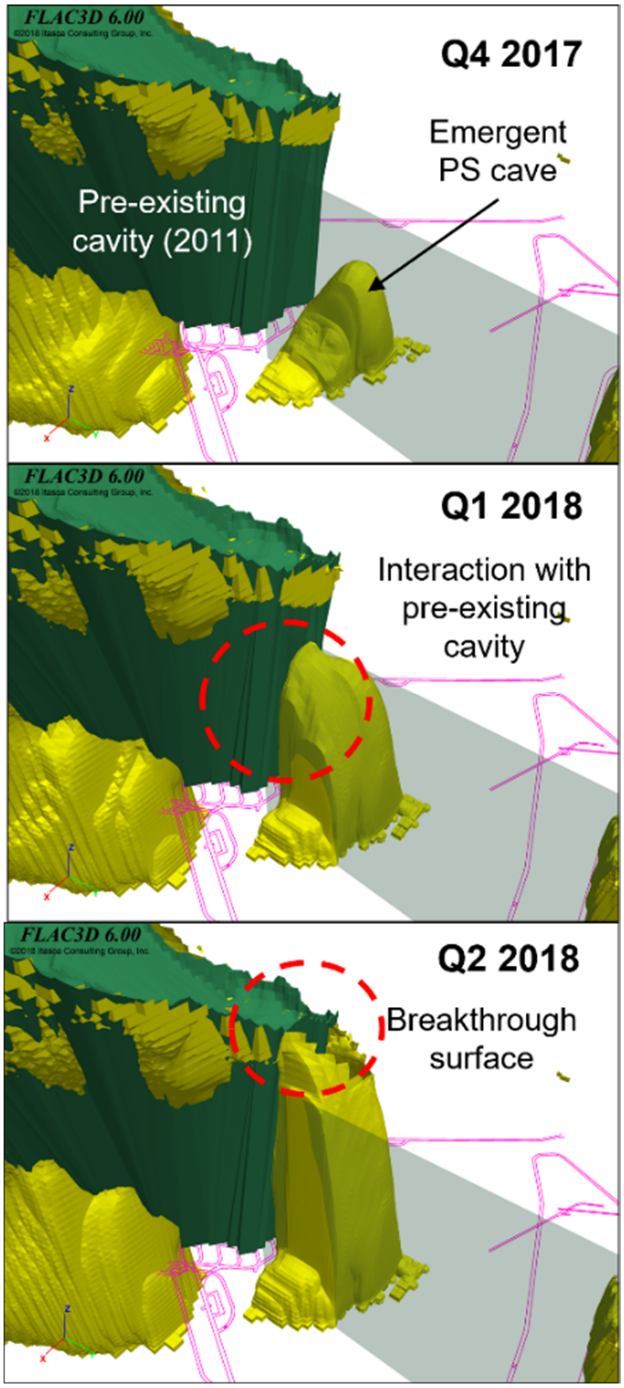

Figure 11 **PS cave propagation for the calibrated model during Q4-2017 and Q2-2018.**

3.4 Subsidence advance

The cave limit capturing the cave advance (see Figure 2) was used to evaluate the subsidence advance, mainly in the area representing the in-situ rock mass condition (above PS panel). On March 9, 2018, a sinkhole was observed on the surface above the PS. The main hypothesis to explain this phenomenon was that the PS cave reached pre-existing productive sectors from 1920, which did not exist in the available mine maps. DET developed an estimated cave shape for the PS considering geological, geotechnical, and seismic parameters, as well as extraction rates and subsidence inspections on site. Also, an area of large deformations (mobilized) was identified and interpreted for better calibration of the model. These geometries were compared to the emergent mobilized limit from the *FLAC3D* model. The model results were controlled by the strength of the Secondary Pipe unit in that sector. The initial simulations overpredicted the subsidence advance and the sinking rate (cratering) above the *Pipa Norte* panel. In order to calibrate the model, the GSI of the Secondary Pipe was increased from 33 to 40 points, achieving an overall good agreement with the cave extension observed by Q3-2018 (sinkhole and large deformation area versus emergent *FLAC3D* cave), and with the sinking rate above the Pipa Norte panel, which was compared with the aero-photogrammetry flights for March 2018 as shown in Figure 12 (cyan color represents nulled elements in the model (i.e., cratering), the topography must be compared with zones in green and gray). Note that the simulation considers the cave mining activity from 2012, calibrating these results after 6.5 years of simulation.

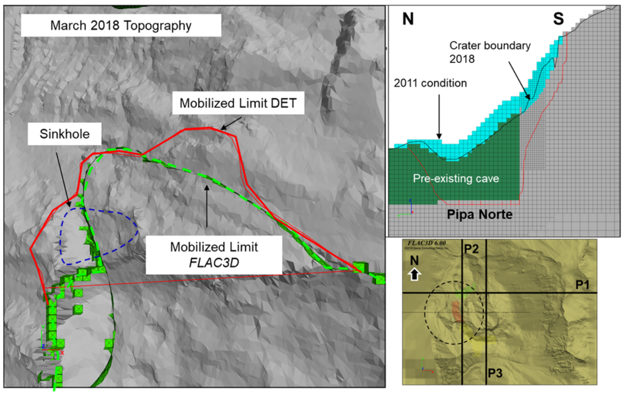

Figure 12 Left: Plan view of the sector above the PS with the area of large deformations in red and the emergent cave shape in green. Right: Comparison between the model and cratering above Pipa Norte.

The pre-existing caves that produced the sinkhole above the PS were not available and not included in the model, which is why the model did not reproduce the cave in that corner. The sinkhole volume was initialized in the model as broken rock to improve predictions.

3.5 Cratering

In this stage, the cratering from the model is compared with the known topography. The cratering was studied using three relevant sections for the open pit project. The results of the calibrated model by Q2 2017 are shown in Figure 13 compared to the topography of April 2017 (latest available at that time). A reasonable agreement was found, with vertical differences between 20 m to 40 m in the area of interest. A mass balance was implemented in the cratering algorithm to account for the failed material filling the bottom of the crater as shown in Figure 14. Similar comparisons were made for intermediate years (2014 and 2015), indicating good agreement with the model.

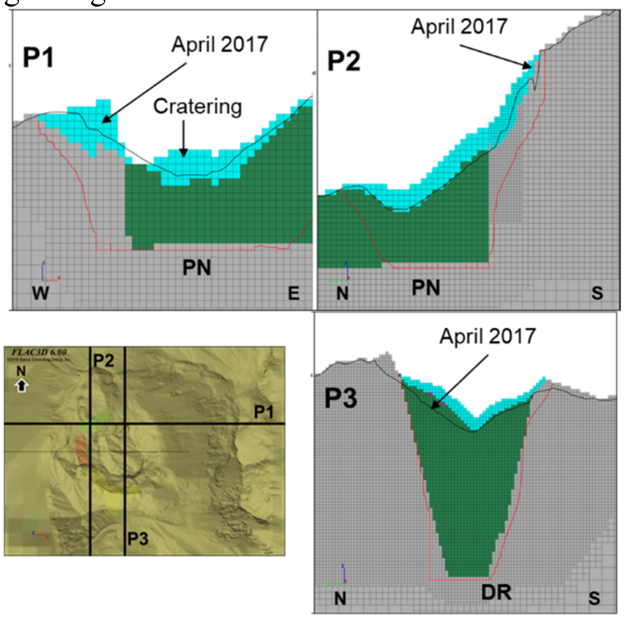

Figure 13 Calibrated cratering results in three sections of interest comparing Q2-2017 condition to April 2017 topography.

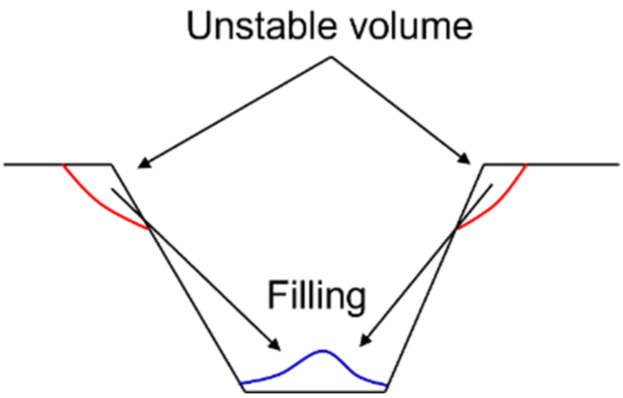

Figure 14 Lateral migration example.

4 MODEL PREDICTIONS

The predictive analysis was carried out using the calibrated model with an extended extraction plan from 2012 to 2025. The results are shown in terms of the subsidence advance (Figure 15) and vertical topographical changes (cratering) in a NS cross-section through the PS panel (Figure 16). The PS cave was predicted to interact with the PN cave in early 2022 in terms of mobilized limits. The emerging cratering and cave shapes were provided to DET as triangulated mesh surfaces for each year of assessment.

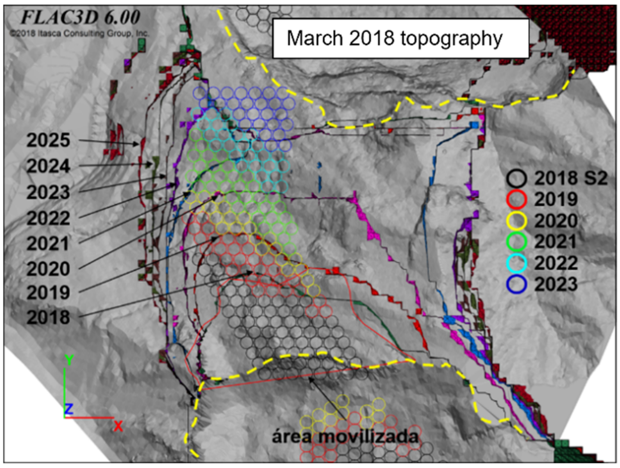

Figure 15 Plan view showing predicted cave advance on surface from 2018 to 2025 above the PS panel.

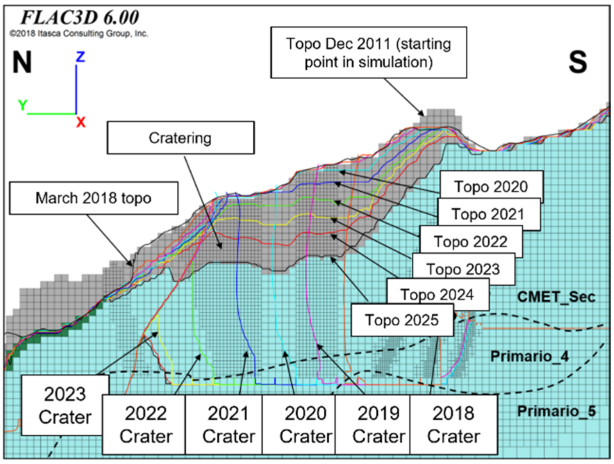

Figure 16 NS cross-section showing predicted surface subsidence from 2018 to 2025 above the PS panel.

4.1 Model Validation

This study was carried out during 2018. After 4 years of active mining, the actual subsidence advance along with the 2022 topography became available. Figure 17 shows the crater boundary for 2022 along with the subsidence advance from the *FLAC3D* model for 2022. The area of interest is above PS panel (around Braden pipe), showing that by 2022, the crater gets connected by PS mining from the south (DR mining) and towards the north (PN mining), in accordance with the result from the *FLAC3D* model.

A comparison of the cratering from *FLAC3D* to the actual 2022 topography is shown in Figure 18 along a NS section across PS. It shows very good agreement toward the north, but not so toward the south (early mining from 2018). It is interesting that the worse agreement is observed at the area where the sinkhole took place in early 2018, with the crater being underestimated. This is likely due to the collapse of voids from early mining, which were not accounted for in the numerical model. The sinkhole from 2018 was an early manifestation of those voids. With that in mind, the comparison could be considered satisfactory. It is worth noting that the predictive production for PS from 2018–2022 is within 3% of the actual production.

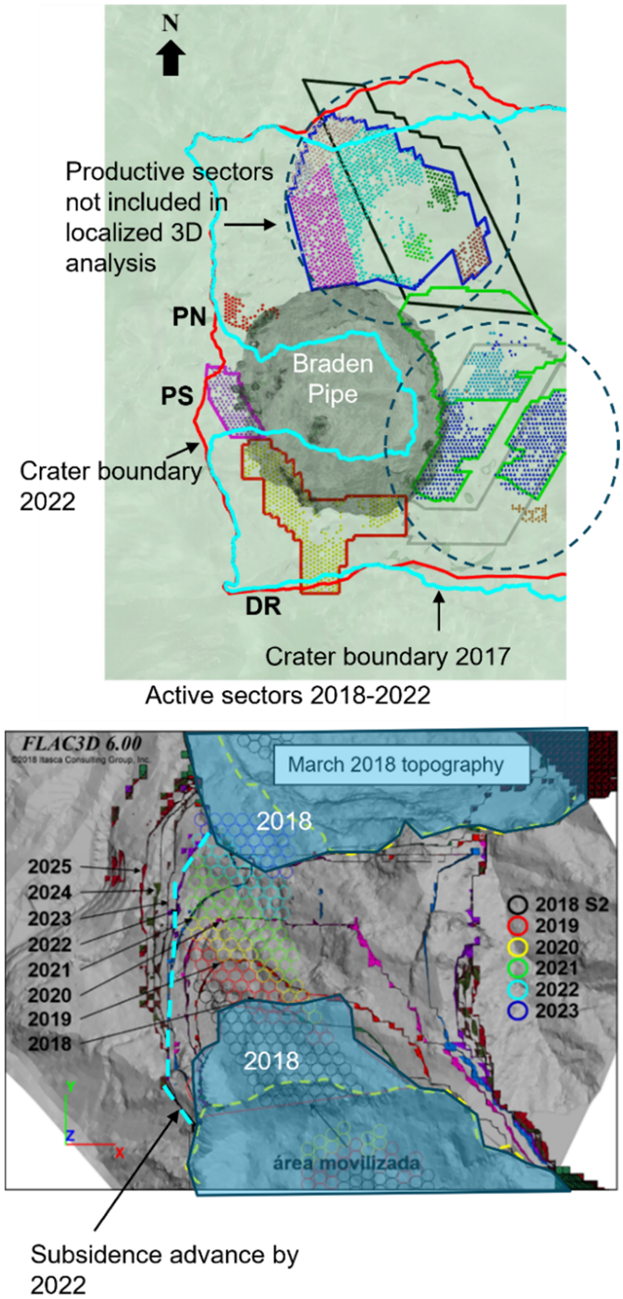

Figure 17 Plan view comparing subsidence advance from *FLAC3D* (right) to field observation (left).

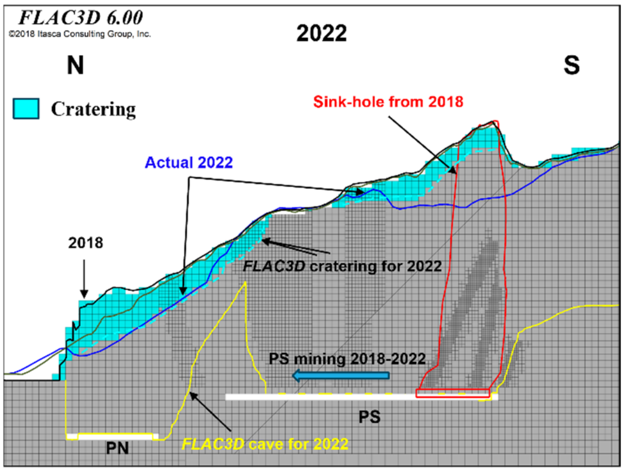

Figure 18 NS cross-section comparing cratering from *FLAC3D* model and actual topography in 2022.

5 NUMERICAL MODELING LIMITATIONS AND IMPROVEMENTS

The performance of numerical models heavily relies on accurate geotechnical characterization. Significant deviations from the initial assumptions can significantly affect model predictions. Uncertainties may stem from rock mass heterogeneity, unmapped faults, and changes in the mining schedule. For instance, the sinkhole observed in 2018 was caused by voids from unrecorded mining activities, highlighting the impact of unaccounted site conditions.

Currently, caving can be modeled within a coupled mechanical and gravitational flow framework using the *FLAC3D-MassFlow* approach, as demonstrated by Cancino et al. (2024). *MassFlow* (Itasca, 2023b) facilitates the modeling of airgaps and rock fragmentation, which are crucial for understanding caveability and subsidence phenomena. Transitioning from annual or semi-annual to monthly evaluation intervals can provide a more granular assessment of cave mine and open pit interactions. This change allows for a more realistic and smoother simulation of cave initiation, propagation, and subsidence processes. Longer evaluation periods in the *FLAC3D-MassFlow* approach may lead to the formation of unrealistic airgaps, which can be mitigated by conducting shorter, more frequent evaluations.

Additionally, adopting the *IMASS* model (Ghazvinian et al., 2020), the predecessor of *Cave-Hoek* model, could enhance the simulation of rock mass behavior. The *IMASS* model's ability to capture post-peak behavior with greater complexity can lead to more accurate predictions and a better understanding of interactions between cave mining and open pit operations.

6 CONCLUSIONS

A subsidence analysis was carried out at El Teniente Mine to assess the possible interaction of the underground operation with the ENRS open pit project.

The caving algorithm was used within *FLAC3D* to simulate cave mining, calibrating the model to past behavior (for the period 2012–2018). After modifying the strength of the primary rock near the PS extraction level and the strength of the Secondary Pipe on surface, an overall good agreement was found compared to site observations in terms of PS cave propagation, crater lateral extension, and vertical topographical changes over time (cratering). The predictions were used by DET to assess and plan the ENRS project. To date, the model predictions made in 2018 show a good overall agreement with actual topographies and estimated cave shapes.

ACKNOWLEDGEMENT

The authors wish to thank the El Teniente Division at CODELCO-Chile for approval to publish this work.

REFERENCES

Alvarez, C., Gomez, P. & Nehgme, P. (2014). Cratering prediction due to block caving, in Proceedings ISRM Specialized Conference 09-13 September, Goiania, Brazil.

Board, M. & Pierce, M. (2009). A review of recent experience in modeling of caving, International Workshop on Numerical Modelling for Underground Mine Excavation Design, June 28, 2009, Asheville, in conjunction with the 43rd US Rock Mechanics Symposium.

Brzovic, A. (2010). Characterization of primary copper ore for block caving at the El Teniente mine, Chile. PhD Thesis, Western Australian School of Mines of Curtin University of Technology.

Cancino, C., Alvarez, C., Gomez, P., Cavieres, P., Jara, R., Figueroa, C. & Millan, J. (2019). Subsidence analysis of waste dumps located inside an active caving crater, in Proceedings of the 14th ISRM Congress on Rock Mechanics, pp. 2974-2986, Iguacu, Brazil.

Cancino, C., Fuenzalida, M. & Kamp, C. (2024). Numerical modeling of cave propagation and breakthrough timing: A back-analysis at New Afton Mine, in Proceedings of the Nineth International Conference and Exhibition on Mass Mining (MassMin 2024, September), Kiruna.

Duplancic, P. & Brady, B. H. (1999). Characterization of caving mechanisms by analysis of seismicity and rock stress, in Proceedings of the 9th ISRM Congress on Rock Mechanics, Vol 2., pp. 1149-1053, Paris, France.

El Teniente Division, 2015. Internal Note GRMD-SGM-NI-110-2015 to Geomechanics Superintendent: Mine Scale Numerical Model of Stresses, El Teniente Division. MVA Geoconsulta.

Ghazvinian, E., Garza-Cruz, T., Bouzeran, L., Fuenzalida, M., Cheng, Z., Cancino, C. & Pierce, M. (2020). Theory and Implementation of the Itasca Constitutive Model for Advanced Strain Softening (IMASS), 8th International Conference & Exhibition on Mass Mining, MassMin 2020, 451–461. Santiago: University of Chile.

Itasca Consulting Group, Inc. (2023a). FLAC3D — Fast Lagrangian Analysis of Continua in Three Dimensions (Version 9.0). Minneapolis: Itasca.

Itasca Consulting Group, Inc. (2023b). MassFlow — A gravity flow simulator (Version 9.0). Minneapolis: Itasca.

Pardo, C. (2015). Back analysis of intensive rock mass damage at the El Teniente mine. PhD Thesis, Western Australian School of Mines of Curtin University of Technology.

Sainsbury, B. (2012). A model for cave propagation and subsidence assessment in jointed rock masses, PhD Thesis, The University of New South Wales, Sydney.